



# Cosmogenic $^{21}\text{Ne}$ exposure ages on late Pleistocene moraines in Lassen Volcanic National Park, California, USA

Joseph P. Tulenko<sup>1,2</sup>, Greg Balco<sup>3,1</sup>, Michael A. Clynne<sup>4</sup>, L.J. Patrick Muffler<sup>4</sup>

<sup>1</sup>Berkeley Geochronology Center, Berkeley, CA, 94709, USA

5 <sup>2</sup>Department of Geology, University at Buffalo, Buffalo, NY, 14260, USA

<sup>3</sup>Lawrence Livermore National Laboratory, Livermore, CA, 94550, USA

<sup>4</sup>USGS Volcano Science Center, Moffett Field, CA, 94035, USA

Correspondence to: Joseph P. Tulenko (jtulenko@bgc.org)

**Abstract.** We report new cosmogenic  $^{21}\text{Ne}$ -in-quartz exposure ages from 18 samples on three distinct moraines deposited in the Lost Creek drainage, approximately 3–7 km down-valley from Lassen Peak in Lassen Volcanic National Park. Although measuring  $^{21}\text{Ne}$  in quartz is generally straightforward, accurate  $^{21}\text{Ne}$  exposure dating of deposits of late Pleistocene-age is rarely possible due to the significant quantities of non-cosmogenic  $^{21}\text{Ne}$  present in most lithologies. Young quartz-bearing volcanic rocks have been observed to be an exception. We take advantage of moraine boulders sourced from the ~28 ka dacite of Lassen Peak to generate a chronology of alpine deglaciation in Lassen Volcanic National Park. Ages from three distinct moraines are in stratigraphic order, ranging ~22–15 ka, and generally agree with other terminal and some recessional moraine ages across the Cascades and Sierra Nevada Range of the western United States. To date, these are among the youngest surfaces ever dated using cosmogenic  $^{21}\text{Ne}$  and provide a cost-effective proof-of-concept approach to dating moraines where applicable.

## 1 Introduction

20 Moraines deposited on the landscape from past alpine glaciers mark the culmination of glacier advances and, when carefully mapped and dated, can record the magnitude and timing of these advances. One of the most effective tools for dating moraines is cosmogenic-nuclide exposure dating because 1) it provides a direct age constraint on the landform, and 2) in many alpine glacier settings, glaciers can be highly erosive. Glacial erosion and transport are important processes that act to both remove cosmogenic nuclides from previously exposed surfaces and expose previously shielded rocks and sediments to the cosmic ray flux at Earth's surface (Balco, 2011). For late Pleistocene-age glaciations, the common target cosmogenic nuclide has been  $^{10}\text{Be}$  for several reasons; 1) it is produced in quartz (which is easily isolated from other minerals and relatively common), 2) its geologically short half-life limits the amount of background  $^{10}\text{Be}$  in fresh rock surfaces, 3) the production of  $^{10}\text{Be}$  on Earth is almost exclusively through cosmic radiation (Gosse and Philips, 2001), and 4) it can reliably be measured at low concentrations. However,  $^{10}\text{Be}$  analyses require time-consuming wet chemical dissolution under clean lab conditions, and costly analytical measurements via Accelerator Mass Spectrometry. In some cases, other cosmogenic

nuclides – particularly noble gas cosmogenic nuclides like  $^{21}\text{Ne}$  and  $^3\text{He}$  – can be used as time-saving and cost-effective alternatives.

35 During glacial periods throughout the late Pleistocene, alpine glaciers and ice caps flowed from numerous high mountain centers in the western United States and deposited detailed sequences of moraines (Palacios et al., 2020). Glacial geologists have extensively dated these moraines in the western US using surface-exposure dating; to date, more than 2100 samples have been analyzed in 85 publications (data pulled from ICE-D, [www.ice-d.org](http://www.ice-d.org); last access 09/20/2023). Moraines deposited during the latest global glacial interval, termed the Last Glacial Maximum (LGM; 26-19 ka, Clark et al., 2009) and subsequent last deglaciation (19-11 ka; Clark et al., 2012) have been thoroughly investigated in several regions in the western US (see Laabs et al., 2020 and references therein). Moraines dated primarily with **surface-exposure** dating have  
40 linked alpine glacial patterns to local and regional climate mechanisms inferred from other climate proxies – including enhanced precipitation inferred from pluvial lakes (Laabs et al., 2009; Quirk et al., 2020), Laurentide Ice Sheet-atmosphere dynamics (Tulenko et al., 2020), and global climate drivers such as atmospheric  $\text{CO}_2$  (Shakun et al., 2015). These observations of past glacier advances, and their linkages to climate change, provide important context for current and future  
45 climate and glacier change.

The Cascades Volcanic Arc, located on the western North American margin, is the product of active subduction of the Juan de Fuca plate below the North American Plate. The arc hosts numerous volcanoes, and volcanism has been active throughout the Pleistocene and Holocene (O'Hara et al., 2020). The detailed history of the Lassen Volcanic Center (herein the LVC) in  
50 Northeastern California (Figs. 1 and 2) – the southernmost active volcano system in the arc – is well documented (Christiansen et al., 2002; Clynne and Muffler, 2010). The most important volcanic deposit for our study is referred to as the dacite of Lassen Peak (further described below), which is the result of the emplacement of a volcanic dome at  **$28.3 \pm 2.7$  ka** (Turrin et al., 1998). The dome was likely glaciated during the LGM as several drainages flowing radially outward from the LVC contain well-preserved sequences of moraines comprised of till dominated by dacite of Lassen Peak (Fig. 2). For this  
55 study, we focus on moraines deposited 3–7 km down-valley on the northern side of Lassen Peak in the Lost Creek drainage (Figs. 2 and 3).



60 **Figure 1. Map of the Cascades and Sierra Nevada region**  
61 **with small stars of other previously investigated sites with**  
62 **glacier chronologies. Wallowa Mountains, OR; Licciardi et**  
63 **al., 2004, White Branch Fault Zone; Alexander et al. (2022),**  
64 **Klamath Lake Fault Zone, OR; Speth et al. (2018), Lake**  
65 **Tahoe Region, CA; Pierce et al. (2017), central Sierra**  
66 **Nevada Range, CA; Rood et al. (2011a, 2011b), southeast**  
67 **Sierra Nevada Range, CA; Benn et al. (2006), Amos et al.**  
68 **(2010). The large yellow star denotes the location of our**  
69 **study site in Lassen Volcanic National Park. Inset: Map of**  
70 **the US and portions of Canada with overlain limits of LGM**  
71 **glaciation in North America from Dalton et al. (2020)**  
72 **outlined and filled in semi-transparent white polygons.**

This paper presents 18 cosmogenic  $^{21}\text{Ne}$ -in-quartz exposure ages from large boulders situated atop three distinct moraines in the Lost Creek drainage of Lassen Volcanic National Park. Although measurements of cosmogenic  $^{21}\text{Ne}$  in quartz by noble gas mass spectrometry are generally straightforward,  $^{21}\text{Ne}$  is rarely used for exposure-dating of LGM-age deposits for two reasons. First, neon extracted from quartz is a mixture of atmospheric and in-situ cosmogenic neon (Niedermann 1993, 2002). Although the two are easily distinguished by their distinct isotopic compositions (see section 3.3), the presence of large amounts of atmospheric neon decreases the precision with which the cosmogenic neon inventory can be measured. For example, concentrations of atmospherically derived  $^{21}\text{Ne}$  in quartz are commonly in the range 50-100 Matoms/g. For a sample with an LGM exposure age and 1 Matom/g of cosmogenic  $^{21}\text{Ne}$ , this means that only 1-2% of the total  $^{21}\text{Ne}$  released is cosmogenic; even if the Ne isotope ratios used to deconvolve atmospheric and cosmogenic inventories are measured with 1% precision, this still leads to a 50% uncertainty on the amount of cosmogenic  $^{21}\text{Ne}$ . Second, quartz in most lithologies contains significant quantities of nucleogenic neon produced as a byproduct of decay of naturally occurring trace U and Th (Niedermann 2002), which, unlike atmospheric neon, cannot be distinguished from cosmogenic neon using the isotopes of neon ( $^{20}\text{Ne}$ ,  $^{21}\text{Ne}$ , and  $^{22}\text{Ne}$ ). Nucleogenic  $^{21}\text{Ne}$  concentrations in quartz of 1-10 Matoms/g are commonly observed in lithologies with cooling ages of more than a few million years (e.g., Balco et al., 2019); at the latitude and altitude of the samples in this study, these concentrations would be equivalent to exposure ages of tens to hundreds of thousands of years. Thus, it is rarely possible to accurately quantify the amount of





cosmogenic  $^{21}\text{Ne}$  produced since the LGM in the presence of a commonly substantially larger nucleogenic and atmospheric background. For this reason, cosmogenic  $^{21}\text{Ne}$  exposure dating has been most applied to deposits with exposure ages of hundreds of thousands to millions of years (Dunai et al., 2005; Balter-Kenney et al., 2020; Spector and Balco, 2021).

100

Although accurate  $^{21}\text{Ne}$ -in-quartz exposure-dating of LGM-age samples is difficult in nearly all rocks, young quartz-bearing volcanic rocks can be an exception, in certain cases. Because the concentration of nucleogenic  $^{21}\text{Ne}$  scales with the cooling age of the rock, nucleogenic  $^{21}\text{Ne}$  concentrations in quartz are expected to be essentially negligible in late Pleistocene volcanics. In addition, quartz in extrusive volcanic rocks has been observed to have low concentrations of included atmospheric neon compared to most rocks (e.g., Phillips et al., 1998; Libarkin et al., 2002; Goethals et al., 2009). Although this observation is largely empirical, it is most likely explained by rapid cooling of eruptive rocks from magmatic temperatures (at which neon is diffusively lost from quartz within minutes) to ambient surface temperatures (at which neon is effectively diffusively immobile). In addition, residence of quartz at magmatic temperatures immediately prior to eruption makes the presence of any trapped magmatic neon with unusual isotopic composition extremely unlikely (Niedermann, 2002). Thus, obstacles to  $^{21}\text{Ne}$  exposure dating that are present in most lithologies are minimized for quartz in late Pleistocene eruptive volcanics.

105

110

For this study, the young age, rapid eruptive nature, and lithology of the Lassen Peak dome provide a unique opportunity to exposure-date young surfaces with cosmogenic  $^{21}\text{Ne}$ . Even though measurement precision for  $^{21}\text{Ne}$  concentrations and resulting ages on LGM deposits are still not as good as for  $^{10}\text{Be}$  ages reported on contemporary moraines deposited in other sites in the Cascades and Sierra Nevada Range, our ages broadly align with these other sites, suggesting we captured the general timing of moraine emplacements in the region, and opening the door for future work dating late Pleistocene moraines with  $^{21}\text{Ne}$ .

115

## 2 Background and Setting

The landscape surrounding Lassen Volcanic National Park is dominated by complex volcanic eruptive sequences ranging in age from 3.5 Ma to present (Clynne and Muffler, 2010; Muffler and Clynne, 2015; Clynne and Muffler, 2017). The latest sequences of volcanic activity, which formed the LVC, began ~825 ka. Since then, there have been three eruptive episodes. The youngest of these episodes, referred to here as the Lassen domefield, began ~315 ka and is currently active. The latest activity occurred in 1914-1917 when a vent at the top of Lassen Peak erupted. The Lassen domefield is further subdivided by both age and lithology (see Fig. 8 in Muffler and Clynne, 2015); we focus on the Eagle Peak sequence (~115 ka – present; Germa et al., 2019) during which Lassen Peak formed. The Eagle Peak sequence describes geologic units from eight distinct eruptions in the park, and one of the youngest and most prominent geologic units is the dacite of Lassen Peak (unit dl in Clynne and Muffler, 2010). Outcrops of the dacite of Lassen Peak in the park are generally restricted to areas near Lassen

125



130 Peak, but boulders, blocks and debris of the dacite are incorporated into expansive surficial deposits, including the  
pyroclastic and debris flows associated with the eruption at Lassen Peak in 1915, late Pleistocene glacial tills draped over the  
landscape near Lassen Peak, and glacial outwash in nearby valleys far down (at least 30 km) from Lassen Peak. Radiometric  
Ar/Ar dating of the unit indicates that the dacite of Lassen Peak was erupted at  $28.3 \pm 2.7$  ka (Turrin et al., 1998). Several  
lines of evidence show that the dome was glaciated during the LGM as well (Turrin et al., 1998; Clynne and Muffler, 2010;  
Fig. 2). Such lines of evidence include abundant moraines and other glacial deposits incorporating sediments and blocks  
135 derived from the dacite of Lassen Peak, and evidence that the mantle of hot, prismatic jointed talus blocks that formed  
the eruptive carapace on Lassen Peak was almost completely stripped by glaciation (Clynne and Muffler, 2010).

The dacite of Lassen Peak is a dome and lithic pyroclastic-flow deposit. The lava dome is a porphyritic dacite with 30%  
phenocrysts of quartz (up to 10%), plagioclase, hornblende, and biotite in a glassy to aphanitic, weakly magnetic  
140 groundmass. The rock also contains small amounts of clinopyroxene and olivine derived from disaggregated mafic  
inclusions. It is the combination of abundant quartz and clinopyroxene that makes dacite of Lassen Peak distinctive among  
other dacites in the Lassen dome field.

Zircon dating and trace-element analysis suggests that the quartz must have been stored at a sub-liquidus temperature in a  
145 'crystal mush' phase between  $\sim 190$  ka and the eruption of Lassen Peak at  $28.3 \pm 2.7$  ka (Klemetti and Clynne, 2014), and  
that the periodic infusion of mafic magma caused the dome eruption and other recent volcanic activity. Given the relatively  
young age of the dacite of Lassen Peak, the volcanic and glacial setting of the LVC, and the abundant availability of quartz  
phenocrysts, we hypothesized that the dacite of Lassen Peak might be a good target for surface-exposure dating of late  
Pleistocene surficial deposits using cosmogenic  $^{21}\text{Ne}$ .

150 Prior to, and following the LVC dome eruption at  $\sim 28$  ka, it is likely that large ice caps smothered the surrounding landscape  
(Fig. 2; Turrin et al., 1998) as global climate transitioned to glacial periods during, for example, Marine Isotope Stage 6 and  
2 (MIS 6; 191–130 ka; MIS 2; 29–11 ka; Lisiecki and Raymo, 2005). Whereas there are no absolute ages on glacial deposits  
in and around the LVC, Clynne and Muffler (2010) summarize previous mapping efforts and subdivide glacial deposits into  
155 'older' and 'younger' tills, where the older tills correlate to the regionally identified Tahoe Glaciation (likely MIS 6; Laabs et  
al., 2020) and the younger tills correlate to the Tioga Glaciation (constrained to MIS 2), known locally as the Anklin  
Meadows glaciation (Turrin et al., 1998). Moraines in several drainages around Lassen Peak have been identified and  
mapped (Turrin et al., 1998; Christiansen et al., 2002), and Anklin Meadows moraines have been subdivided largely by their  
elevation, stratigraphic position, and the presence/absence of known age lithologies comprising the sediments and blocks  
160 embedded in the moraines.

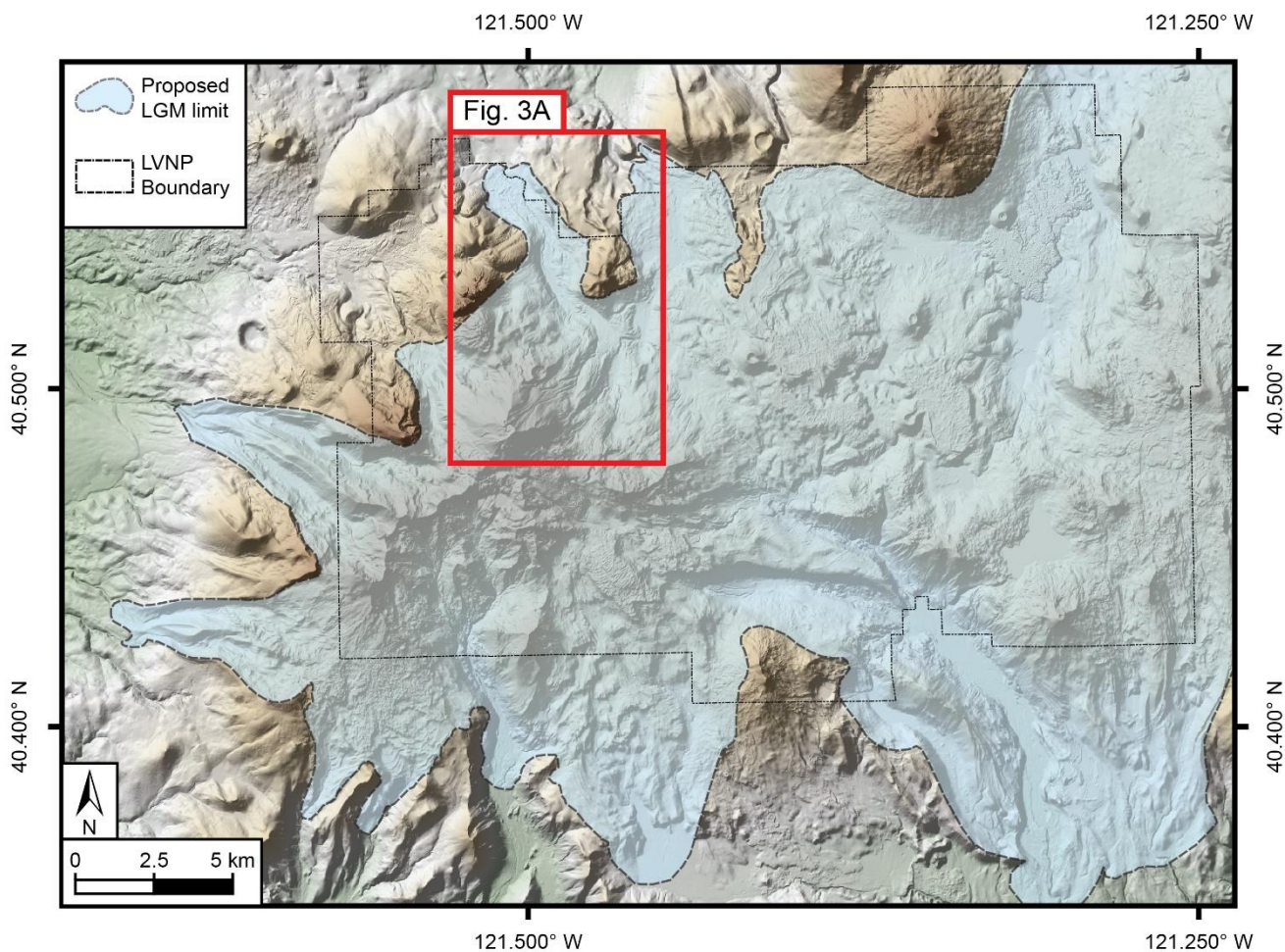


Figure 2. Map of Lassen Volcanic National Park and vicinity. Dot-dot-dash lines are park boundary, light blue transparent shade is the proposed limit of LGM glaciation in the region (adapted from Clynne and Muffler, 2010). Basemap and hillshade are from the 1/3 arc-second digital elevation model made available through the USGS National Map 3D Elevation Program (<https://www.usgs.gov/programs/national-geospatial-program/national-map> date of last access; Feb 1, 2024).

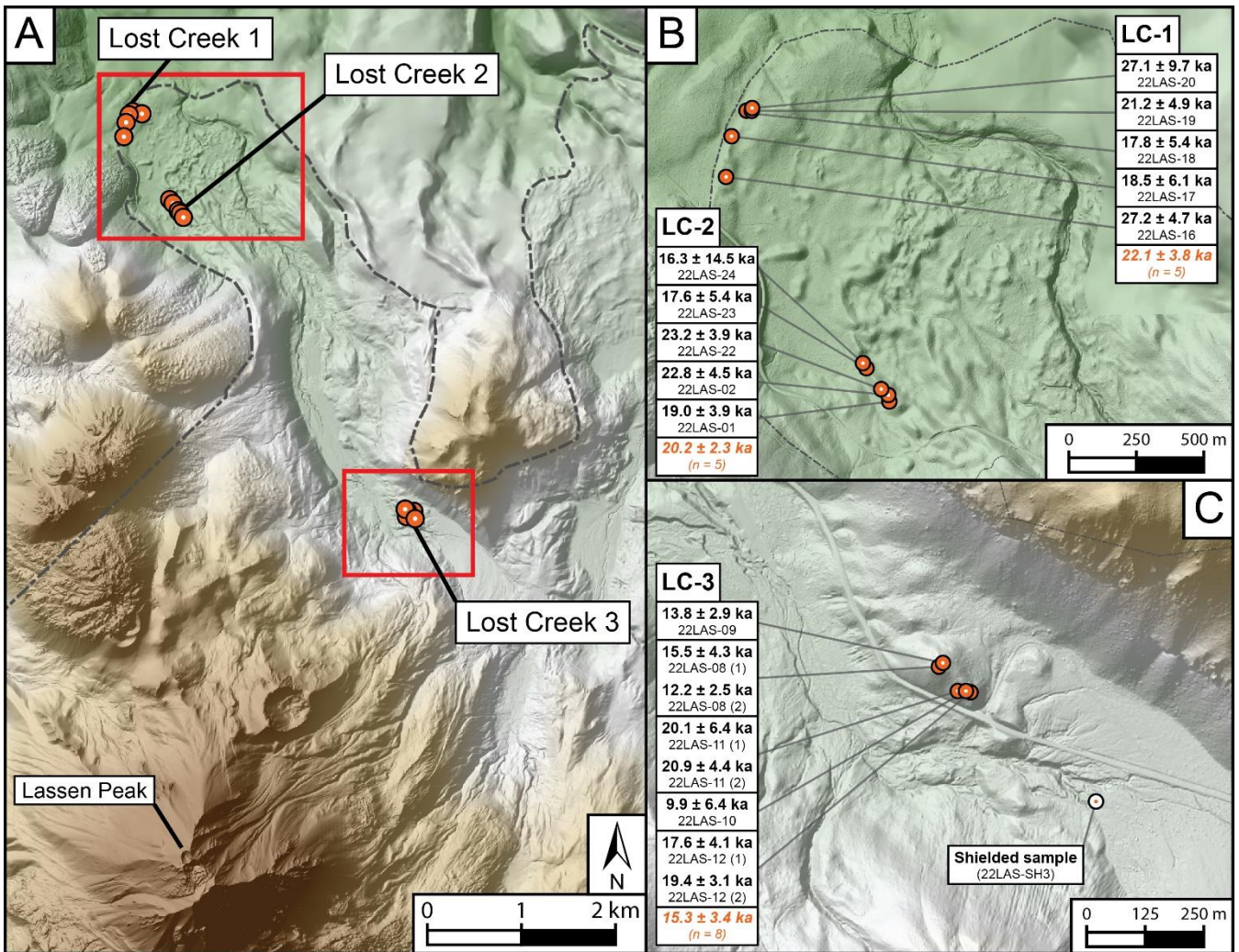
165

Turrin et al. (1998, and later updated in Clynne and Muffler, 2010), described several sets of Anklin Meadows moraine units in Lost Creek drainage (Fig. 3); we targeted moraines mapped from the two oldest units, Anklin Meadows A1 and A2. The oldest and lowest-elevation moraines (Anklin Meadows A1) are found around 1600-1700 m asl in Lost Creek drainage. Anklin Meadows A2 moraines were deposited around 1950 m asl. Below, we describe two moraines mapped within the A1 unit (Lost Creek Moraine 1 and Lost Creek Moraine 2; Fig. 3A and 3B), and one moraine mapped within the A2 unit (Lost Creek Moraine 3; Fig. 3A and 3C). All moraines in the Lost Creek drainage contain abundant boulders up to 4 m in diameter of dacite of Lassen Peak transported by ice that flowed from Lassen Peak down-valley. In the Lost Creek drainage, large avalanche and debris flow deposits from the 1915 eruption (which include entrained massive blocks sourced from the dacite

170



of Lassen Peak) follow the center of the drainage, but these deposits did not override the moraines that we targeted for exposure dating (Christiansen et al., 2002).  
 175



180  
 185  
**Figure 3.** Lost Creek drainage north of Lassen Peak. A). A: Complete Lost Creek drainage with sample locations highlighted for each moraine (Lost Creek 1, 2 and 3). B: Zoom in on Lost Creek 1 and Lost Creek 2 (A1) moraines. Samples listed with calculated ages and internal uncertainties. Average moraine ages in orange text. C: Zoom in on Lost Creek moraine 3 (A2) up-valley from Lost Creek moraines 1 and 2. Individual ages and moraine ages reported in the same way as panel B. Note the multiple aliquots measured for samples 22LAS-08, 22LAS-11 and 22LAS-12. Location of the large block entrained in the 1915 avalanche and debris flow used to procure a shielded sample noted in panel C. Basemap and hillshade are sourced from post-processed, Lidar-based digital elevation model products available through the USGS National Map 3D Elevation Program (<https://www.usgs.gov/programs/national-geospatial-program/national-map> date of last access; Feb 1, 2024).



### 3 Materials and methods

#### 3.1 Sample collection and processing

We collected surface samples for cosmogenic  $^{21}\text{Ne}$  exposure dating from 15 boulders sourced from the dacite of Lassen Peak on the crests of three distinct moraines in the Lost Creek drainage in summer 2022. We sampled five boulders on each moraine. We targeted large (1–2 m tall; Fig. 4; see [www.ice-d.org](http://www.ice-d.org) for all field sample photos) tabular boulders with low-sloping top surfaces to limit the impact of surface erosion. In addition to reduced snow cover from wind-sweeping, the tops of large boulders are also better shielded from forest fire activity, which has the potential to heat surfaces to the point where  $^{21}\text{Ne}$  can diffuse out of quartz (Shuster and Farley, 2005). We extracted approximately 1 kg of sample from the surface of each boulder using a carbide tipped power drill, steel wedges, and a hammer. We recorded longitude and latitude using a handheld GPS and calculated topographic- and self-shielding corrections using in-field measurements with a smartphone app clinometer and the shielding correction calculator from the online exposure age calculator website (<https://hess.ess.washington.edu/>).

**Table 1. Field observations and analytical measurements for sampled boulders**

| Sample name          | Latitude (DD) | Longitude (DD) | Elevation (m a.s.l.) | Sample thickness (cm) | Shielding Correction | quartz weight (g) | Ne-21 TOT (atoms $10^6$ ) | Ne-21 excess (atoms $10^6$ ) | Ne-21 excess (%) | [Ne-21 excess] (atoms/g $10^6$ ) | Ne-21 exposure age (ka) |
|----------------------|---------------|----------------|----------------------|-----------------------|----------------------|-------------------|---------------------------|------------------------------|------------------|----------------------------------|-------------------------|
| Lost Creek Moraine 1 |               |                |                      |                       |                      |                   |                           |                              |                  |                                  |                         |
| 22LAS-16             | 40.56015      | -121.51479     | 1718                 | 1.0                   | 1.000000             | 0.2952            | 1.14 ± 0.08               | 0.517 ± 0.09                 | 45.4             | 1.75 ± 0.306                     | 27.2 ± 4.7              |
| 22LAS-17             | 40.56150      | -121.51450     | 1713                 | 1.0                   | 1.000000             | 0.4647            | 2.53 ± 0.15               | 0.552 ± 0.182                | 21.9             | 1.187 ± 0.392                    | 18.5 ± 6.1              |
| 22LAS-18             | 40.56234      | -121.51382     | 1711                 | 2.0                   | 1.000000             | 0.3992            | 1.86 ± 0.12               | 0.45 ± 0.137                 | 24.2             | 1.127 ± 0.344                    | 17.8 ± 5.4              |
| 22LAS-19             | 40.56235      | -121.51363     | 1713                 | 1.5                   | 1.000000             | 0.4933            | 2.27 ± 0.13               | 0.669 ± 0.155                | 29.4             | 1.356 ± 0.314                    | 21.2 ± 4.9              |
| 22LAS-20             | 40.56243      | -121.51358     | 1712                 | 2.0                   | 1.000000             | 0.2757            | 2.45 ± 0.15               | 0.483 ± 0.173                | 19.7             | 1.751 ± 0.628                    | 27.1 ± 9.7              |
| Lost Creek Moraine 2 |               |                |                      |                       |                      |                   |                           |                              |                  |                                  |                         |
| 22LAS-01             | 40.55251      | -121.50780     | 1767                 | 2.5                   | 1.000000             | 0.4990            | 2.15 ± 0.11               | 0.615 ± 0.126                | 28.5             | 1.232 ± 0.252                    | 19.0 ± 3.9              |
| 22LAS-02             | 40.55272      | -121.50785     | 1768                 | 2.0                   | 1.000000             | 0.4131            | 1.68 ± 0.11               | 0.627 ± 0.122                | 37.4             | 1.517 ± 0.296                    | 22.8 ± 4.5              |
| 22LAS-22             | 40.55292      | -121.50816     | 1764                 | 2.0                   | 1.000000             | 0.4417            | 1.33 ± 0.09               | 0.613 ± 0.102                | 46.2             | 1.387 ± 0.231                    | 23.2 ± 3.9              |
| 22LAS-23             | 40.55364      | -121.50880     | 1754                 | 2.0                   | 1.000000             | 0.2638            | 1.16 ± 0.08               | 0.298 ± 0.09                 | 25.6             | 1.129 ± 0.343                    | 17.6 ± 5.4              |
| 22LAS-24             | 40.55379      | -121.50892     | 1753                 | 2.0                   | 1.000000             | 0.4711            | 6.9 ± 0.34                | 0.487 ± 0.433                | 7.1              | 1.033 ± 0.919                    | 16.3 ± 14.5             |
| Lost Creek           |               |                |                      |                       |                      |                   |                           |                              |                  |                                  |                         |



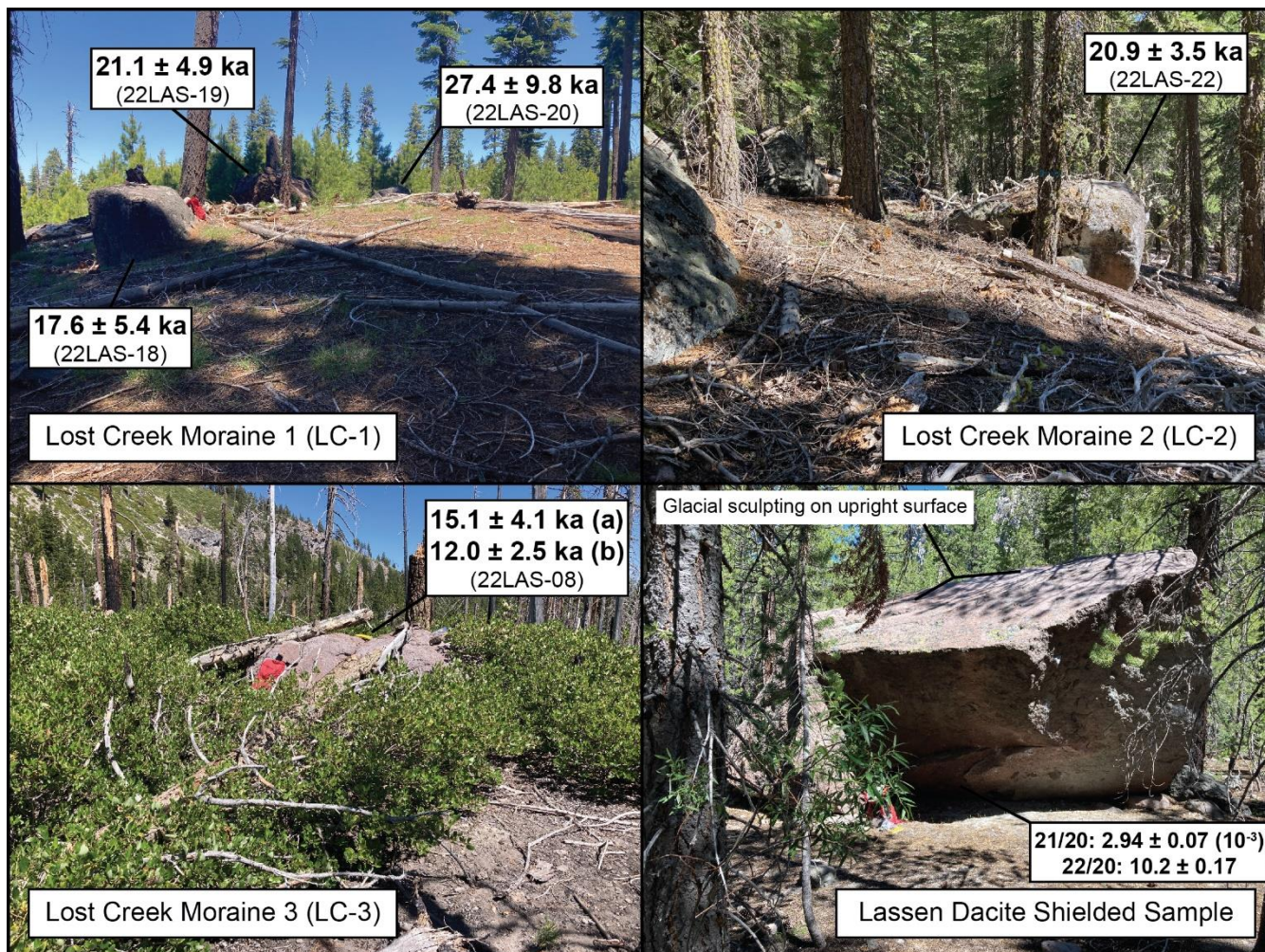


|   |              |                    |      |     |              |        |             |                  |                     |               |            |
|---|--------------|--------------------|------|-----|--------------|--------|-------------|------------------|---------------------|---------------|------------|
| Moraine 3                                   |              |                    |      |     |              |        |             |                  |                     |               |            |
| 22LAS-08 (a)                                | 40.52<br>369 | -<br>121.48<br>016 | 1950 | 3.0 | 0.99256<br>8 | 0.4085 | 1.61 ± 0.11 | 0.457 ±<br>0.126 | 28.4                | 1.12 ± 0.308  | 15.5 ± 4.3 |
| 22LAS-08 (b)                                | -            | -                  | -    | -   | -            | 0.4240 | 1.33 ± 0.07 | 0.378 ±<br>0.077 | 28.4                | 0.892 ± 0.182 | 12.2 ± 2.5 |
| 22LAS-09                                    | 40.52<br>376 | -<br>121.48<br>004 | 1950 | 1.0 | 0.99256<br>8 | 0.5300 | 1.73 ± 0.1  | 0.535 ±<br>0.112 | 30.9                | 1.009 ± 0.212 | 13.8 ± 2.9 |
| 22LAS-10                                    | 40.52<br>318 | -<br>121.47<br>945 | 1941 | 1.5 | 0.99256<br>8 | 0.4875 | 3.16 ± 0.19 | 0.359 ±<br>0.232 | 11.4                | 0.736 ± 0.476 | 9.9 ± 6.4  |
| 22LAS-11 (a)                                | 40.52<br>319 | -<br>121.47<br>965 | 1939 | 1.5 | 0.99256<br>8 | 0.4462 | 2.41 ± 0.15 | 0.524 ±<br>0.177 | 21.8                | 1.174 ± 0.396 | 20.1 ± 6.4 |
| 22LAS-11 (b)                                | -            | -                  | -    | -   | -            | 0.4282 | 3.7 ± 0.11  | 0.668 ± 0.14     | 18.1                | 1.561 ± 0.326 | 20.9 ± 4.4 |
| 22LAS-12 (a)                                | 40.52<br>316 | -<br>121.47<br>933 | 1942 | 2.0 | 0.99256<br>8 | 0.3804 | 1.59 ± 0.1  | 0.49 ± 0.113     | 30.8                | 1.287 ± 0.298 | 17.6 ± 4.1 |
| 22LAS-12 (b)                                | -            | -                  | -    | -   | -            | 0.4063 | 1.81 ± 0.08 | 0.582 ±<br>0.093 | 32.2                | 1.433 ± 0.228 | 19.4 ± 3.1 |
| dacite of Lassen<br>Peak Shielded<br>Sample |              |                    |      |     |              |        |             |                  |                     |               |            |
| 22LAS-SH3                                   | -            | -                  | -    | -   | -            | 0.4567 | 4.02 ± 0.21 | not detected     | not<br>detecte<br>d | not detected  | -          |

200 **Notes: all samples are sourced from the dacite of Lassen Peak, thus sample density assumed to be 2.80 g/cm<sup>3</sup> for all samples. Three samples (22LAS-08, 22LAS-11, and 22LAS-12) that have two aliquots measured on each are labeled with (a) and (b) to distinguish aliquots. All additional neon measurements and analyses are reported in the supplementary table S1.**

We also procured a sample from the underside of a large (>5m tall) block of dacite of Lassen Peak entrained in the 1915  
 205 avalanche and debris flow in the Lost Creek drainage, for the purpose of constraining the nucleogenic component of <sup>21</sup>Ne-  
 excess (see below). The upward-facing surface of the large tabular block displayed evidence of glacial sculpting (Fig. 4; e.g.,  
 striations), so we interpret that the top of the block was exposed after deglaciation, plucked, and entrained in the avalanche  
 and debris flow during the 1915 eruption and deposited glacially sculpted side up. Thus, it is likely that the underside of the  
 block where we sampled was completely shielded from the cosmic-ray flux following formation and through the eruption,  
 plucking, and deposition process.

210



215 Figure 4. Example field sample photos, one per moraine. Clockwise from top left: Three samples clustered nearby on the outermost LGM moraine, Lost Creek 1, one boulder embedded in the Lost Creek 2 moraine, the large block sourced from the dacite of Lassen Peak that was entrained in the 1915 avalanche and debris flow with approximate location of underside sample collection noted, and one boulder with two aliquots measured from the collected surface sample on the Lost Creek 3 moraine. Moraine boulders are shown with calculated ages and internal uncertainties.

We prepared all samples, including the ‘shielded’ sample, at the Berkeley Geochronology Center rock preparation lab and then the University at Buffalo cosmogenic isotope lab. We crushed sample fractions of approximately 150 g from each total sample (sample thicknesses reported here are the thicknesses of the sample fractions that were crushed) using a mortar and pestle and sieved to 300-600 microns. We rinsed this target fraction and separated magnetic minerals using a Frantz magnetic separator, leaving quartz and plagioclase. To isolate quartz from plagioclase, we used the froth flotation method (see Corbett et al., 2016) before etching the quartz-rich fractions in low-concentration HF to remove any remaining plagioclase and the outside of the quartz grains that may have been enriched in nucleogenic  $^{21}\text{Ne}$  derived from alpha implantation through U/Th decay in adjacent minerals or glass (see Niedermann, 2002 for more details).

220



## 225 3.2 Analytical measurements

We measured all three neon isotopes ( $^{20}\text{Ne}$ ,  $^{21}\text{Ne}$ ,  $^{22}\text{Ne}$ ) in purified quartz on the “Ohio” noble gas mass spectrometer (NGMS) system at the Berkeley Geochronology Center. The NGMS system consists of a MAP-215 sector field mass spectrometer with modernized ion-counting electronics coupled to a fully automated gas extraction system. We encapsulated ~0.4 g aliquots of quartz in tantalum packets and heated them under vacuum using a 150W, 810 nm diode laser, in two  
230 heating steps at 950° C and 1200° C. Reactive gases were removed by exposure to a SAES Getter, remaining noble gases were frozen to an activated charcoal trap at 33 K, non-adsorbed gases (presumably mostly He) were pumped away, and Ne was released to the mass spectrometer at 75 K.

All three isotopes of neon were measured by ion-counting, with corrections for  $\text{CO}_2^{++}$  on mass 22 and  $^{40}\text{Ar}^{++}$  on mass 20  
235 made using an  $^{39}\text{Ar}$  spike (Balco and Shuster, 2009). Absolute Ne concentrations are determined by peak height comparison with an air standard measured several times daily. Mass discrimination corrections are also based on the air standard. Reported uncertainties include counting uncertainties on all masses (including those used for correction of isobars), correction for an extraction line “cold” blank measured without any introduction of sample, and the reproducibility of the air standard. “Hot” blanks that included heating of empty metal packets released small amounts of neon with atmospheric  
240 isotope composition, so this contribution is accounted for in the calculation of excess  $^{21}\text{Ne}$  and a separate hot blank correction was not made. The amount and isotopic composition of neon released in all 1200° C steps was indistinguishable from that released in the hot blanks, so we conclude that the samples were fully degassed at 950° C, and report only the results of the first heating steps. Three aliquots of the **CRONUS-A standard** analyzed during the period of this study yielded excess  $^{21}\text{Ne}$  concentrations of  $336.1 \pm 8.1$  Matoms/g. This is slightly more than the nominal value for this standard of 320  
245 Matoms/g (Vermeesch et al., 2015). Although in Table 1 we report data as measured, excess  $^{21}\text{Ne}$  concentrations are renormalized to the nominal value of 320 when calculating exposure ages, as described below.

## 3.3 Cosmogenic $^{21}\text{Ne}$ measurements and age calculations

From the measured neon isotope results we then calculated excess  $^{21}\text{Ne}$  as follows:

$$^{21}\text{Ne}_{xs} = ^{21}\text{Ne}_{tot} - (Ra_{21/20} * ^{20}\text{Ne}_{tot})$$

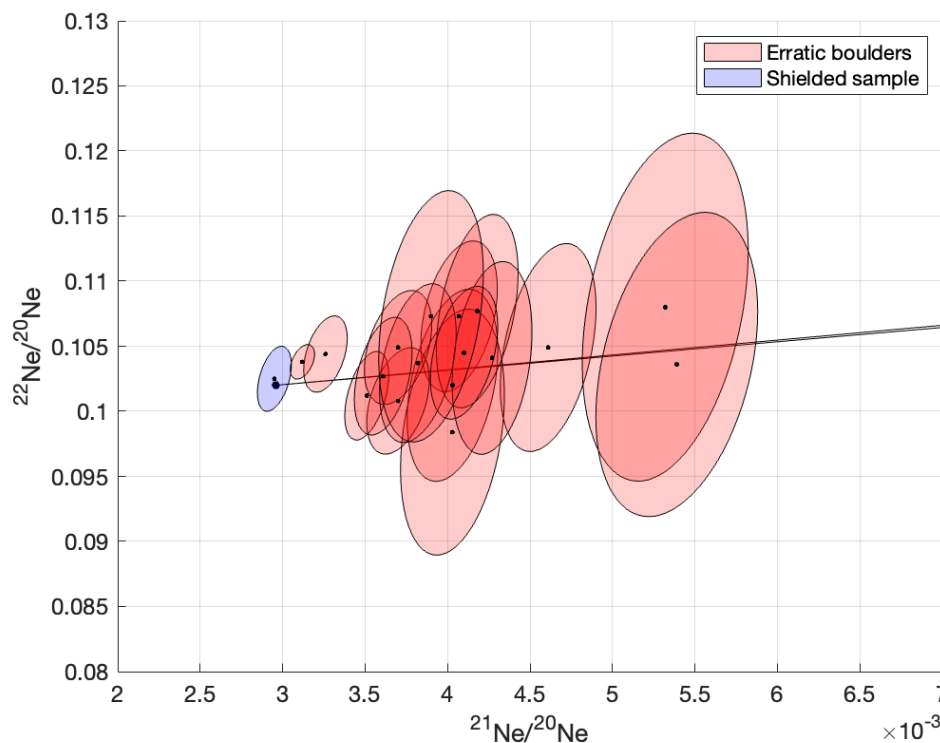
250 Where  $^{21}\text{Ne}_{xs}$  is excess  $^{21}\text{Ne}$  relative to atmosphere,  $Ra_{21/20}$  is the atmospheric  $^{21}\text{Ne}/^{20}\text{Ne}$  ratio (0.002959),  $^{21}\text{Ne}_{tot}$  is total measured  $^{21}\text{Ne}$ , and  $^{20}\text{Ne}_{tot}$  is total measured  $^{20}\text{Ne}$ . As shown below in the results (and in the supplementary table), excess  $^{21}\text{Ne}$  in the shielded sample was indistinguishable from zero, so we take excess  $^{21}\text{Ne}$  to be equivalent to cosmogenic  $^{21}\text{Ne}$ . We then computed cosmogenic  $^{21}\text{Ne}$  exposure ages using version 3 of the online exposure age calculator described by Balco et al. (2008) and subsequently updated, with the LSDn scaling method (Lifton et al., 2014, 2016) and production rate  
255 calibration data from the SPICE project in Arizona, USA (Fenton et al., 2019). As mentioned above, exposure-age calculations in the online calculator include normalization to the nominal value of 320 Matoms/g for CRONUS-A. Further,

we assume negligible post-depositional boulder surface erosion and snow cover as a common community practice, which means that all ages presented here are minimum exposure ages.

#### 4 Results

260 As hypothesized, quartz in the dacite of Lassen Peak has an undetectable amount of nucleogenic  $^{21}\text{Ne}$  and unusually low concentrations of atmospheric neon. First,  $^{21}\text{Ne}/^{20}\text{Ne}$  and  $^{22}\text{Ne}/^{20}\text{Ne}$  ratios in the shielded sample are  $0.00294 \pm 0.0007$  and  $0.1025 \pm 0.0017$ , respectively, which are indistinguishable from atmosphere (Figure 5). This implies that nucleogenic  $^{21}\text{Ne}$  in quartz in this lithology is negligible and, in addition, provides no evidence for the presence of any trapped magmatic neon. Thus, as noted above, we calculated excess  $^{21}\text{Ne}$  to be equivalent to cosmogenic  $^{21}\text{Ne}$ . Second, concentrations of atmospheric neon in quartz in this lithology, expressed as  $^{21}\text{Ne}$ , are  $4.4 \pm 3.0$  Matoms/g  $^{21}\text{Ne}$  (mean and standard deviation of all samples), which, although still greater than concentrations of cosmogenic  $^{21}\text{Ne}$  in the 0.75-1.5 Matoms/g range, are substantially lower than in most other measured rocks to date.

265



270 **Figure 5.** Neon three-isotope plot for all 950° C heating steps. The black dot is the composition of atmospheric neon, and the black line is the atmospheric-cosmogenic mixing line. The ellipses are 68% confidence regions. The isotope composition of neon in the shielded sample is indistinguishable from atmosphere, indicating a negligible concentration of nucleogenic or magmatic neon. All other data lie on or near the atmospheric-cosmogenic mixing line within uncertainty.



Cosmogenic  $^{21}\text{Ne}$  concentrations in moraine boulder samples in the Lost Creek drainage range from  $\sim 0.736 - 1.751$  Matoms/g and account for  $\sim 27 \pm 9\%$  of the total measured  $^{21}\text{Ne}$  in each sample (Table 1), with the remaining fraction being attributable to atmospheric  $^{21}\text{Ne}$ . Calculated  $^{21}\text{Ne}$  exposure ages for all samples range from  $27.1 \pm 9.7$  ka to  $9.9 \pm 6.4$  ka (Table 1; Figure 6). Ages from each moraine comprise single populations. On the outermost terminal LGM moraine (LC-1), 5 ages from 5 boulders **average  $22.1 \pm 3.8$  ka** (moraine ages reported here and throughout are the arithmetic mean and one standard deviation, without propagating an additional production rate uncertainty). A few hundred meters up-valley, 5 ages from 5 boulders on the next dated moraine (LC-2) **average  $20.2 \pm 2.3$  ka**. Finally, 4 km up-valley from LC-1 and LC-2, **8 ages from 5 boulders (with replicate measurements on 22LAS-08, 22LAS-11, and 22LAS-12) from the innermost recessional moraine dated in the Lost Creek Drainage (LC-3) average  $15.3 \pm 3.4$  ka**. Thus, ages for the three moraines are in stratigraphic order.

285

**Figure 6. Individual probability density functions (pdfs) for each sample (green) and summed pdfs for each moraine age (black). Individual pdfs are based on the calculated age and internal uncertainty for each sample. Blue bars indicate the mean and 1 standard deviation of the ages on each moraine.**

## 295 5 Discussion

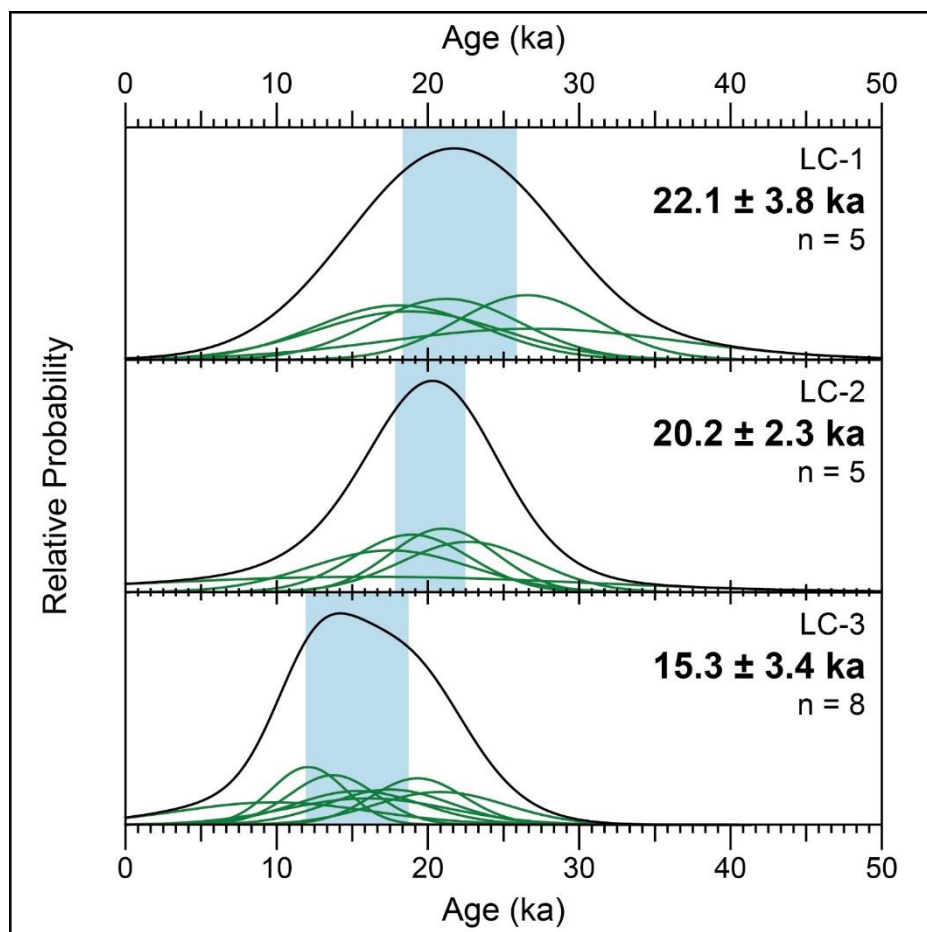
We now assess 1) the efficacy of the dating method itself for late Pleistocene deposits and 2) the power of resolving local glacial and climate histories based on the results.

300

### 5.1 Cosmogenic $^{21}\text{Ne}$ exposure dating of the dacite of Lassen Peak

305

Our initial hypothesis, that due to the relatively young age and rapid rate of cooling of the dacite of



Lassen Peak the nucleogenic and atmospheric  $^{21}\text{Ne}$  concentrations in this lithology are relatively low, is supported by the measurements. This demonstrates that the dacite of Lassen Peak is a favorable target for  $^{21}\text{Ne}$  exposure dating.

310

Although this is not the first study to take advantage of the low  $^{21}\text{Ne}$  background in young quartz-bearing volcanic rocks (for example, see work on the Bandelier Tuff in New Mexico, USA by Phillips et al., 1998), to the best of our knowledge, the moraines described here are the youngest landforms successfully exposure-dated using  $^{21}\text{Ne}$  to date in any published study. However, although the dacite of Lassen Peak is among the best-case scenarios for dating recently exposed surfaces with cosmogenic  $^{21}\text{Ne}$ , we still find that a majority of the total  $^{21}\text{Ne}$  inventory is non-cosmogenic (Table 1), which limits the precision of the dating method. This is especially true in comparison with  $^{10}\text{Be}$  measurements that produce uncertainties up to an order of magnitude lower than those reported here, 2-3% versus ~20-30%. However, considering the total cost of analyses and preparation time for  $^{10}\text{Be}$  measurements – which can be up to an order of magnitude more expensive – cosmogenic  $^{21}\text{Ne}$ , in unique situations like these, might be a suitable avenue to efficiently test broad generalized hypotheses and provide a proof-of-concept for further, more detailed investigation with higher-precision techniques.

320

## 5.2 Deglacial history of the LVC in the context of the broader Cascades and Sierra Nevada Range region

Moraine ages in Lost Creek indicate that the LGM may have culminated in LVNP ca. 22 ka (LC-1), with ice remaining near the maximum extent for another ~2 kyr, to emplace a recessional moraine (LC-2) ca. 20 ka. There are additional moraines and hummocky terrain just inboard of the LC-2 moraine that have not yet been sampled, but an additional dated recessional moraine (LC-3) ~4 km up-valley indicates ~4 km of modest recession, then deposition of a moraine at ca. 15 ka.

325

We next compare our record of deglaciation in LVNP with a subset of all other sites ( $n = 13$ ) around the Cascades and Sierra Nevada Range, summarized in Figure 7. All data extracted for this comparison come from the ICE-D database (www.ice-d.org; last access: 09/01/2023; citations to the original data generators noted in each figure panel). Sites were identified specifically as moraines in the region with a minimum of four ages per moraine to increase the likelihood that ages compared reflect a true glacier termination and not other processes (e.g., boulder exhumation/moraine degradation). For each moraine, we systematically identified extreme values/outliers by calculating the  $\chi^2$  statistic assuming a normal distribution. If the calculated p value – based on the  $\chi^2$  statistic and degrees of freedom per moraine – was below 0.1, we systematically pruned the individual sample with the most extreme individual  $\chi^2$  value until the dataset satisfied the criteria for a normal distribution. Then we simply calculated the mean and standard deviation to estimate the moraine age and uncertainty.

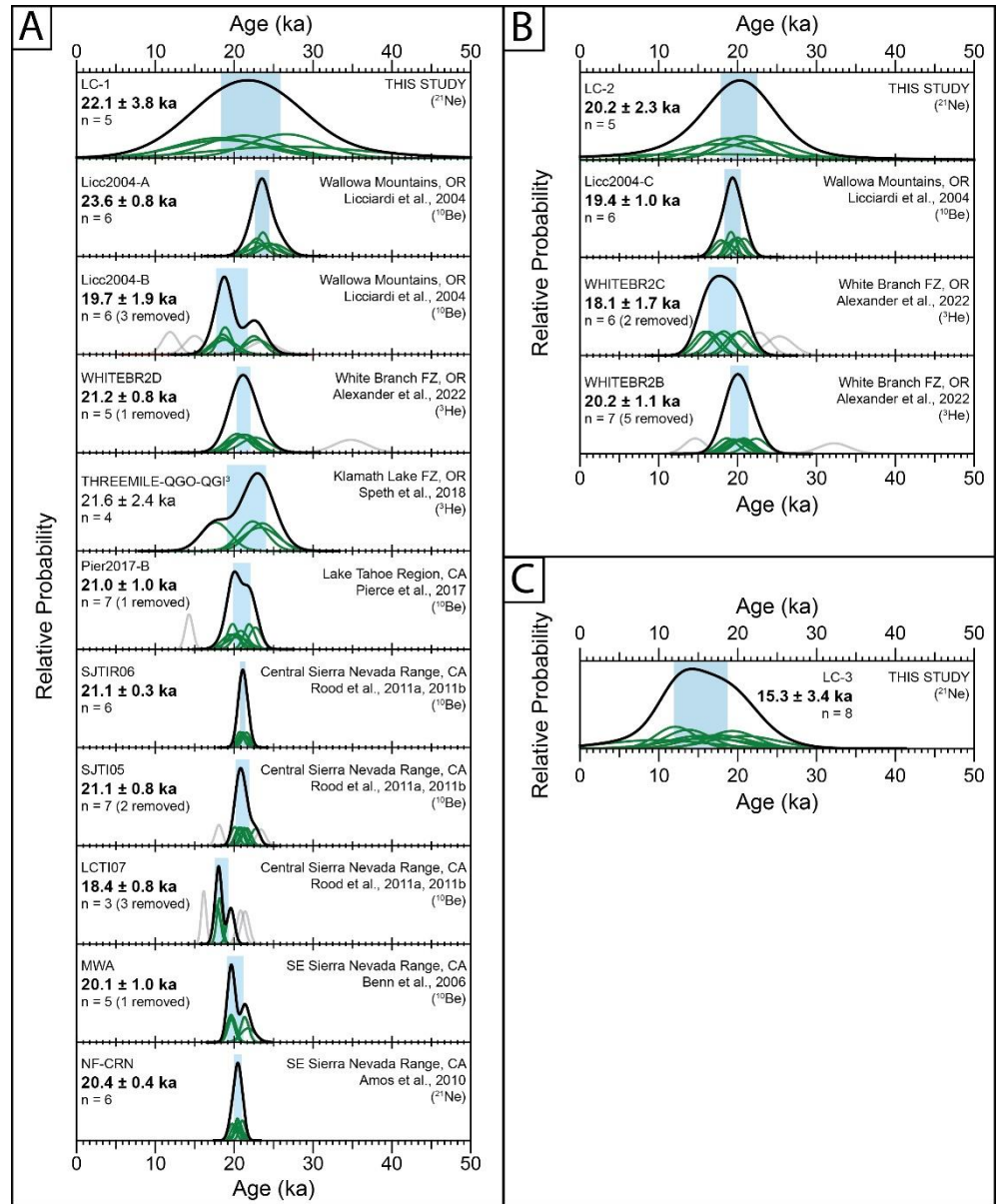
335



340 **Figure 7. Individual and summed pdfs for moraines dated across the Cascades and Sierra Nevada Range. A) Terminal LGM moraine ages from the region listed from North to South (except for the terminal moraine from this study, LC-1, which is listed at the top), B) earliest recessional moraine ages in the region listed North to South, and C) the youngest recessional moraine dated in the LVC (LC-3). For each summed pdf, site (moraine) names from ICE-D, average ages, sample counts (excluding identified outliers noted in parentheses) and citations are reported. Individual ages included in the average age calculation are based on sample ages and internal uncertainties (like Fig. 6) and are plotted in green. Samples that were identified and excluded as outliers using an outlier rejection scheme are plotted in light grey. The solid black line is the summed pdf after outlier removal. The blue box in each plot is the mean and 1 standard deviation of all samples for each moraine. Note that site locations here correspond to site locations and citations denoted in Figure 1.**

375 Terminal LGM moraine ages across the region range ~23 to 18 ka, conforming with our

21Ne-based moraine ages, within error. Moreover, a handful of the other sites around the region contain dated recessional moraines ranging ~20 to 19 ka that also conform well with our LC-2 moraine. Thus, it is possible that whatever regional climatic controls acted on alpine glacial patterns in other sites across the region were also acting on the glaciers in the LVC. However, additional late Pleistocene recessional moraines to compare with the inner recessional moraine dated in Lost Creek drainage (LC-3) are not currently observed in the region. It is unclear whether this dearth is due to climatic forcing inhibiting moraine deposition at other sites during this time, the lack of preservation of similar recessional moraines in other valleys, or a lack of surveying and sampling, all of which currently remain unresolved. It is notable, however, that in other parts of the





385 western US, such as the central Colorado Rockies (e.g., Schweinsberg et al., 2020) and the Pioneer Mountains in SW  
Montana (Schoenemann et al., 2023), there is evidence of moraine deposition ca. ~15-16 ka, coinciding with timing of LC-3  
moraine deposition at our site. Whether this is a result of regional climate or local factors in the LVC, higher-precision  
measurements and further investigation at our study site are required to resolve these new questions.

## 6 Conclusions

390 We present 18 new cosmogenic  $^{21}\text{Ne}$  exposure ages on three distinct, inset moraines in Lassen Volcanic National Park, NE  
California that average  $22.1 \pm 3.8$  ka ( $n = 5$ ),  $20.2 \pm 2.3$  ka ( $n = 5$ ), and  $15.3 \pm 3.4$  ka ( $n = 8$ ) on each respective moraine.  
Although the precision of our  $^{21}\text{Ne}$  exposure ages is approximately an order of magnitude lower than ages from other sites in  
the region, individual moraine ages that we measured are distinguishable and in stratigraphic order. The moraine ages  
indicate that the LGM may have culminated in LVNP in-step with other glaciated valleys across the Cascades and Sierra  
395 Nevada Range, with a notable exception for the youngest moraine, LC-3, that appears to be unique to the LVC when  
compared to other sites in the Cascades and Sierra Nevada Range region. The results from this study present an example of  
an efficient and cost-effective means of estimating moraine ages using  $^{21}\text{Ne}$  in quartz that could be further applied in the  
LVC and in other - likely limited - glaciated regions where quartz-bearing late Pleistocene-age volcanic rocks are present.  
Going forward, this approach may be employed - when targeting glaciated, young volcanic lithologies - as an initial  
400 surveying step in the process of generating precise deglacial records useful for reconstructing glacial and climate processes.

## Author contributions

JPT: Conceptualization, Formal Analysis, Investigation, Data Curation, Writing – Original Draft, Visualization, GB:  
Conceptualization, Investigation, Data Curation, Writing – Review and Editing, Visualization, Funding Acquisition, MAC:  
405 Conceptualization, Investigation, Writing – Review and Editing, LJPM: Conceptualization, Writing – Review and Editing.

## Competing Interests

At least one of the (co-)authors is a member of the editorial board of Geochronology.

## Acknowledgements

We would like to thank the National Park Service in LVNP for permitting us to sample boulders within park boundaries, and  
410 Marie Bergelin for assistance with neon analyses at BGC. JPT was supported by NSF Grant number 1948416. The Berkeley  
Geochronology Center is supported in part by the Ann and Gordon Getty Foundation. Any use of trade, firm, or product





names is for descriptive purposes only and does not imply endorsement by the U.S. Government. Finally, we would like to acknowledge that samples were collected in the Lost Creek drainage on ancestral lands of the Atsugewi, and we give thanks to the original caretakers of these lands.

## 415 **References**

- Alexander, K. A., Amos, C. B., Balco, G., Amidon, W. H., Clark, D. H., Meigs, A. J., and Lesnau, R. K.: Implications of glacial deposit ages for the timing and rate of active crustal faulting in the central Cascade arc, Oregon, USA, *Geosphere*, 18, 1726–1751, <https://doi.org/10.1130/GES02476.1>, 2022.
- 420 Amos, C. B., Kelson, K. I., Rood, D. H., Simpson, D. T., and Rose, R. S.: Late Quaternary slip rate on the Kern Canyon fault at Soda Spring, Tulare County, California, *Lithosphere*, 2, 411–417, <https://doi.org/10.1130/L100.1>, 2010.
- Balco, G.: Contributions and unrealized potential contributions of cosmogenic-nuclide exposure dating to glacier chronology, 1990–2010, *Quaternary Science Reviews*, 30, 3–27, <https://doi.org/10.1016/j.quascirev.2010.11.003>, 2011.
- 425 Balco, G. and Shuster, D. L.: Production rate of cosmogenic  $^{21}\text{Ne}$  in quartz estimated from  $^{10}\text{Be}$ ,  $^{26}\text{Al}$ , and  $^{21}\text{Ne}$  concentrations in slowly eroding Antarctic bedrock surfaces, *Earth and Planetary Science Letters*, 281, 48–58, <https://doi.org/10.1016/j.epsl.2009.02.006>, 2009.
- 430 Balco, G., Stone, J. O., Lifton, N. A., and Dunai, T. J.: A complete and easily accessible means of calculating surface exposure ages or erosion rates from  $^{10}\text{Be}$  and  $^{26}\text{Al}$  measurements, *Quaternary geochronology*, 3, 174–195, <https://doi.org/10.1016/j.quageo.2007.12.001>, 2008.
- Balco, G., Blard, P.-H., Shuster, D. L., Stone, J. O., and Zimmermann, L.: Cosmogenic and nucleogenic  $^{21}\text{Ne}$  in quartz in a  
435 28-meter sandstone core from the McMurdo Dry Valleys, Antarctica, *Quaternary Geochronology*, 52, 63–76, <https://doi.org/10.1016/j.quageo.2019.02.006>, 2019.
- Balter-Kennedy, A., Bromley, G., Balco, G., Thomas, H., and Jackson, M. S.: A 14.5-million-year record of East Antarctic Ice Sheet fluctuations from the central Transantarctic Mountains, constrained with cosmogenic  $^3\text{He}$ ,  $^{10}\text{Be}$ ,  $^{21}\text{Ne}$ , and  $^{26}\text{Al}$ ,  
440 *The Cryosphere*, 14, 2647–2672, <https://doi.org/10.5194/tc-14-2647-2020>, 2020.

Benn, D. I., Owen, L. A., Finkel, R. C., and Clemmens, S.: Pleistocene lake outburst floods and fan formation along the eastern Sierra Nevada, California: implications for the interpretation of intermontane lacustrine records, *Quaternary Science Reviews*, 25, 2729–2748, <https://doi.org/10.1016/j.quascirev.2006.02.018>, 2006.

445

Christiansen, R. L., Clynne, M. A., and Muffler, L. J. P.: Geologic map of the Lassen Peak, Chaos Crags, and Upper Hat Creek area, California, US Geological Survey, 2002.

Clark, P. U., Dyke, A. S., Shakun, J. D., Carlson, A. E., Clark, J., Wohlfarth, B., Mitrovica, J. X., Hostetler, S. W., and McCabe, A. M.: The last glacial maximum, *science*, 325, 710–714, <https://doi.org/10.1126/science.1172873>, 2009.

450

Clark, P. U., Shakun, J. D., Baker, P. A., Bartlein, P. J., Brewer, S., Brook, E., Carlson, A. E., Cheng, H., Kaufman, D. S., and Liu, Z.: Global climate evolution during the last deglaciation, *Proceedings of the National Academy of Sciences*, 109, E1134–E1142, <https://doi.org/10.1073/pnas.1116619109>, 2012.

455

Clynne, M. A. and Muffler, L. J. P.: Geologic map of Lassen Volcanic National Park and vicinity, California, US Geological Survey Scientific Investigations Map 2899, scale 1:50,000., 2010.

Clynne, M.A., and Muffler, L.J.P.: Geologic field-trip guide to the Lassen segment of the Cascades Arc, northern California: U.S. Geological Survey Scientific Investigations Report 2017–5022–K2, 65 p., <https://doi.org/10.3133/sir20175022K2>, 2017.

460

Corbett, L. B., Bierman, P. R., and Rood, D. H.: An approach for optimizing in situ cosmogenic  $^{10}\text{Be}$  sample preparation, *Quaternary Geochronology*, 33, 24–34, <https://doi.org/10.1016/j.quageo.2016.02.001>, 2016.

465

Dalton, A. S., et al.: An updated radiocarbon-based ice margin chronology for the last deglaciation of the North American Ice Sheet Complex, *Quaternary Science Reviews*, 234, 106223, <https://doi.org/10.1016/j.quascirev.2020.106223>, 2020.

Dunai, T. J., López, G. A. G., and Juez-Larré, J.: Oligocene–Miocene age of aridity in the Atacama Desert revealed by exposure dating of erosion-sensitive landforms, *Geology*, 33, 321–324, <https://doi.org/10.1130/G21184.1>, 2005.

470

Fenton, C. R., Niedermann, S., Dunai, T., and Binnie, S. A.: The SPICE project: Production rates of cosmogenic  $^{21}\text{Ne}$ ,  $^{10}\text{Be}$ , and  $^{14}\text{C}$  in quartz from the 72 ka SP basalt flow, Arizona, USA, *Quaternary Geochronology*, 54, 101019, <https://doi.org/10.1016/j.quageo.2019.101019>, 2019.

475



- Germa, A., Perry, C., Quidelleur, X., Calvert, A., Clynne, M., Connor, C. B., Connor, L. J., Malservisi, R., and Charbonnier, S.: Temporal relationship between the Lassen volcanic center and mafic regional volcanism, *Bulletin of Volcanology*, 81, 1–17, <https://doi.org/10.1007/s00445-019-1296-7>, 2019.
- 480 Goethals, M., Niedermann, S., Hetzel, R., and Fenton, C.: Determining the impact of faulting on the rate of erosion in a low-relief landscape: A case study using in situ produced  $^{21}\text{Ne}$  on active normal faults in the Bishop Tuff, California, *geomorphology*, 103, 401–413, <https://doi.org/10.1016/j.geomorph.2008.07.008>, 2009.
- Gosse, J. C. and Phillips, F. M.: Terrestrial in situ cosmogenic nuclides: theory and application, *Quaternary Science*  
485 *Reviews*, 20, 1475–1560, [https://doi.org/10.1016/S0277-3791\(00\)00171-2](https://doi.org/10.1016/S0277-3791(00)00171-2), 2001.
- Klemetti, E. W. and Clynne, M. A.: Localized rejuvenation of a crystal mush recorded in zircon temporal and compositional variation at the Lassen Volcanic Center, Northern California, *PloS one*, 9, e113157, <https://doi.org/10.1371/journal.pone.0113157>, 2014.
- 490 Laabs, B. J., Refsnider, K. A., Munroe, J. S., Mickelson, D. M., Applegate, P. J., Singer, B. S., and Caffee, M. W.: Latest Pleistocene glacial chronology of the Uinta Mountains: support for moisture-driven asynchrony of the last deglaciation, *Quaternary Science Reviews*, 28, 1171–1187, <https://doi.org/10.1016/j.quascirev.2008.12.012>, 2009.
- 495 Laabs, B. J. C., Licciardi, J. M., Leonard, E. M., Munroe, J. S., and Marchetti, D. W.: Updated cosmogenic chronologies of Pleistocene mountain glaciation in the western United States and associated paleoclimate inferences, *Quaternary Science Reviews*, 242, 106427, <https://doi.org/10.1016/j.quascirev.2020.106427>, 2020.
- 500 Libarkin, J.C., Quade, J., Chase, C.G., Poths, J. and McIntosh, W.: Measurement of ancient cosmogenic  $^{21}\text{Ne}$  in quartz from the 28 Ma Fish Canyon Tuff, Colorado. *Chemical Geology*, 186(3-4), pp.199-213, [https://doi.org/10.1016/S0009-2541\(01\)00411-9](https://doi.org/10.1016/S0009-2541(01)00411-9), 2002.
- Licciardi, J. M., Clark, P. U., Brook, E. J., Elmore, D., and Sharma, P.: Variable responses of western US glaciers during the last deglaciation, *Geology*, 32, 81–84, <https://doi.org/10.1130/G19868.1>, 2004.
- 505 Lifton, N., Sato, T., and Dunai, T. J.: Scaling in situ cosmogenic nuclide production rates using analytical approximations to atmospheric cosmic-ray fluxes, *Earth and Planetary Science Letters*, 386, 149–160, <https://doi.org/10.1016/j.epsl.2013.10.052>, 2014.



- 510 Lifton, N.: Implications of two Holocene time-dependent geomagnetic models for cosmogenic nuclide production rate scaling, *Earth and Planetary Science Letters*, 433, 257–268, <https://doi.org/10.1016/j.epsl.2015.11.006>, 2016.
- Lisiecki, L. E. and Raymo, M. E.: A Pliocene-Pleistocene stack of 57 globally distributed benthic  $\delta^{18}\text{O}$  records, *Paleoceanography*, 20, <https://doi.org/10.1029/2004PA001071>, 2005.
- 515 Muffler, L. P. and Clynne, M. A.: Geologic field-trip guide to Lassen Volcanic National Park and vicinity, California, US Geological Survey Scientific Investigations Report 2015-5067, 67 p., <https://doi.org/10.3133/sir20155067>, 2015.
- Niedermann, S., Graf, T., and Marti, K.: Mass spectrometric identification of cosmic-ray-produced neon in terrestrial rocks with multiple neon components, *Earth and Planetary Science Letters*, 118, 65–73, [https://doi.org/10.1016/0012-821X\(93\)90159-7](https://doi.org/10.1016/0012-821X(93)90159-7), 1993.
- 520 Niedermann, S.: Cosmic-ray-produced noble gases in terrestrial rocks: dating tools for surface processes, *Reviews in mineralogy and geochemistry*, 47, 731–784, <https://doi.org/10.2138/rmg.2002.47.16>, 2002.
- 525 O’Hara, D., Karlstrom, L., and Ramsey, D. W.: Time-evolving surface and subsurface signatures of Quaternary volcanism in the Cascades arc, *Geology*, 48, 1088–1093, <https://doi.org/10.1130/G47706.1>, 2020.
- Palacios, D., Stokes, C. R., Phillips, F. M., Clague, J. J., Alcalá-Reygosa, J., Andrés, N., Angel, I., Blard, P.-H., Briner, J. P., and Hall, B. L.: The deglaciation of the Americas during the Last Glacial Termination, *Earth-Science Reviews*, 203, 103113, <https://doi.org/10.1016/j.earscirev.2020.103113>, 2020.
- 530 Phillips, W. M., McDonald, E. V., Reneau, S. L., and Poths, J.: Dating soils and alluvium with cosmogenic  $^{21}\text{Ne}$  depth profiles: case studies from the Pajarito Plateau, New Mexico, USA, *Earth and Planetary Science Letters*, 160, 209–223, [https://doi.org/10.1016/S0012-821X\(98\)00076-4](https://doi.org/10.1016/S0012-821X(98)00076-4), 1998.
- 535 Pierce, I. K. D., Wesnousky, S. G., and Owen, L. A.: Terrestrial cosmogenic surface exposure dating of moraines at Lake Tahoe in the Sierra Nevada of California and slip rate estimate for the West Tahoe Fault, *Geomorphology*, 298, 63–71, <https://doi.org/10.1016/j.geomorph.2017.09.030>, 2017.
- 540 Quirk, B. J., Moore, J. R., Laabs, B. J., Plummer, M. A., and Caffee, M. W.: Latest Pleistocene glacial and climate history of the Wasatch Range, Utah, *Quaternary Science Reviews*, 238, 106313, <https://doi.org/10.1016/j.quascirev.2020.106313>, 2020.



545 Rood, D. H., Burbank, D. W., and Finkel, R. C.: Chronology of glaciations in the Sierra Nevada, California, from  $^{10}\text{Be}$  surface exposure dating, *Quaternary Science Reviews*, 30, 646–661, <https://doi.org/10.1016/j.quascirev.2010.12.001>, 2011a.

Rood, D. H., Burbank, D. W., and Finkel, R. C.: Spatiotemporal patterns of fault slip rates across the Central Sierra Nevada frontal fault zone, *Earth and Planetary Science Letters*, 301, 457–468, <https://doi.org/10.1016/j.epsl.2010.11.006>, 2011b.

550

Schoenemann, S. W., Bryant, M. M., Larson, W. B., Corbett, L. B., and Bierman, P. R.: A cosmogenic  $^{10}\text{Be}$  moraine chronology of arid, alpine Late Pleistocene glaciation in the Pioneer Mountains of Montana, USA, *Quaternary Science Reviews*, 317, 108283, <https://doi.org/10.1016/j.quascirev.2023.108283>, 2023.

555 Schweinsberg, A. D., Briner, J. P., Licciardi, J. M., Shroba, R. R., and Leonard, E. M.: Cosmogenic  $^{10}\text{Be}$  exposure dating of Bull Lake and Pinedale moraine sequences in the upper Arkansas River valley, Colorado Rocky Mountains, USA, *Quaternary Research*, 97, 125–139, <https://doi.org/10.1017/qua.2020.21>, 2020.

560 Shakun, J. D., Clark, P. U., He, F., Lifton, N. A., Liu, Z., and Otto-Bliesner, B. L.: Regional and global forcing of glacier retreat during the last deglaciation, *Nature Communications*, 6, 1–7, <https://doi.org/10.1038/ncomms9059>, 2015.

Shuster, D. L. and Farley, K. A.: Diffusion kinetics of proton-induced  $^{21}\text{Ne}$ ,  $^3\text{He}$ , and  $^4\text{He}$  in quartz, *Geochimica et Cosmochimica Acta*, 69, 2349–2359, <https://doi.org/10.1016/j.gca.2004.11.002>, 2005.

565 Spector, P. and Balco, G.: Exposure-age data from across Antarctica reveal mid-Miocene establishment of polar desert climate, *Geology*, 49, 91–95, <https://doi.org/10.1130/G47783.1>, 2021.

Speth, G. T., Amos, C. B., Amidon, W. H., Balco, G., Meigs, A. J., and Graf, S.: Glacial chronology and slip rate on the west Klamath Lake fault zone, Oregon, *GSA Bulletin*, 131, 444–460, <https://doi.org/10.1130/B31961.1>, 2018.

570

Tulenko, J. P., Lofverstrom, M., and Briner, J. P.: Ice sheet influence on atmospheric circulation explains the patterns of Pleistocene alpine glacier records in North America, *Earth and Planetary Science Letters*, 534, 116115, <https://doi.org/10.1016/j.epsl.2020.116115>, 2020.

575 Turrin, B. D., Christiansen, R. L., Clynne, M. A., Champion, D. E., Gerstel, W. J., Muffler, L. J. P., and Trimble, D. A.: Age of Lassen Peak, California, and implications for the ages of late Pleistocene glaciations in the southern Cascade Range,



Geological Society of America Bulletin, 110, 931–945, [https://doi.org/10.1130/0016-7606\(1998\)110<0931:AOLPCA>2.3.CO;2](https://doi.org/10.1130/0016-7606(1998)110<0931:AOLPCA>2.3.CO;2), 1998.

580 Vermeesch, P., Balco, G., Blard, P.-H., Dunai, T. J., Kober, F., Niedermann, S., Shuster, D. L., Strasky, S., Stuart, F. M., and Wieler, R.: Interlaboratory comparison of cosmogenic  $^{21}\text{Ne}$  in quartz, Quaternary Geochronology, 26, 20–28, <https://doi.org/10.1016/j.quageo.2012.11.009>, 2015.